

# Structure of a Glutathione Conjugate Bound to the Active Site of Aldose Reductase

Ranvir Singh,<sup>1</sup> Mark A. White,<sup>1,2</sup> Kota V. Ramana,<sup>1</sup> J. Mark Petrash,<sup>3</sup> Stanley J. Watowich,<sup>1,2</sup> Aruni Bhatnagar,<sup>4</sup> and Satish K. Srivastava<sup>1,\*</sup>

<sup>1</sup>Department of Biochemistry and Molecular Biology, University of Texas Medical Branch, Galveston, Texas

<sup>2</sup>Sealy Center for Structural Biology, University of Texas Medical Branch, Galveston, Texas

<sup>3</sup>Department of Ophthalmology, Washington University, St. Louis, Missouri

<sup>4</sup>Institute of Molecular Cardiology, University of Louisville, Louisville, Kentucky

**ABSTRACT** Aldose reductase (AR) is a monomeric NADPH-dependent oxidoreductase that catalyzes the reduction of aldehydes, ketones, and aldoses. AR has been linked to the development of hyperglycemic injury and is a clinical target for the treatment of secondary diabetic complications. In addition to reducing glucose, AR is key regulator of cell signaling through its reduction of aldehydes derived from lipoproteins and membrane phospholipids. AR catalyzes the reduction of glutathione conjugates of unsaturated aldehydes with higher catalytic efficiency than free aldehydes. The X-ray structure of human AR holoenzyme in complex with the glutathione analogue S-(1,2-dicarboxyethyl) glutathione (DCEG) was determined at a resolution of 1.94 Å. The distal carboxylate group of DCEG's dicarboxyethyl moiety interacted with the conserved AR anion binding site residues Tyr48, His110, and Trp111. The bound DCEG's glutathione backbone adopted the low-energy Y-shape form. The C-terminal carboxylate of DCEG glutathione's glycine formed hydrogen bonds to Leu301 and Ser302, while the remaining interactions between DCEG and AR were hydrophobic, permitting significant flexibility of the AR and glutathione (GS) analogue interaction. The observed conformation and interactions of DCEG with AR were consistent with our previously published molecular dynamics model of glutathionyl-propanal binding to AR. The current structure identifies major interactions of glutathione conjugates with the AR active-site residues. *Proteins* 2006;64:101–110. © 2006 Wiley-Liss, Inc.

**Key words:** aldo-keto reductase; competitive inhibitor; active site; diabetic complications; crystal structure; glutathiolation

## INTRODUCTION

Aldose reductase (AR)<sup>1</sup> is a monomeric ( $\alpha/\beta_8$ -barrel (TIM barrel; see Ref. 57) protein [see Fig. 2(A)], which belongs to the aldo-keto reductase (AKR) superfamily.<sup>1–3</sup> It catalyzes the reduction of a structurally diverse range of aldehydes, including aldo-sugars such as glucose, as well as aldehyde metabolites of neurotransmitters, isocorticosteroids, and a variety of xenobiotic aldehydes.<sup>4</sup> Reduction of glucose to sorbitol by AR constitutes the first and

rate-limiting step of the polyol pathway that reduces glucose to sorbitol. Sorbitol is further metabolized to fructose via sorbitol dehydrogenase. Conversion of glucose to osmotically active sorbitol represents an important osmoregulatory mechanism in the renal medulla.<sup>5</sup> In most other tissues, however, the polyol pathway is a minor route of glucose metabolism.<sup>4</sup> Nevertheless, activation of this pathway in hyperglycemic states results in multiple metabolic and signaling changes that have been linked to the development of cataract, nephropathy, neuropathy, and retinopathy, as well as the cardiovascular complications of diabetes mellitus.<sup>4,7,8</sup> Several chemically diverse drugs that inhibit AR have been shown to prevent diabetic changes in nerve, kidney, and lens of experimental animals, although clinical trials with type 1 and type 2 diabetics have not been uniformly positive.<sup>4–8</sup> While there may be several factors confounding the clinical effects of AR inhibitors, a key feature may be the ability of the enzyme to reduce aldehydes other than glucose. Hence, concurrent inhibition of aldehyde detoxification could limit the efficacy of inhibiting AR-dependent glucose metabolism. It is, therefore, critical to understand the role of AR in aldehyde detoxification as it relates to glucose metabolism as well as the regulation of intracellular signaling.

Extensive kinetic and metabolic studies show that AR catalyzes the reduction of potentially toxic aldehydes

*Abbreviations:* AR, aldose reductase, E.C. 1.1.1.21; AKRs, aldo-keto reductases; DCEG, S-(1,2-dicarboxyethyl) glutathione,  $\gamma$ -glutamyl-S-(1,2-dicarboxyethyl) cysteinylglycine; GS, glutathione; RMSD, root-mean-square deviation; HNE, 4-hydroxy *trans*-2-nonenal.

The Supplementary Material referred to in this article can be found at <http://www.interscience.wiley.com/jpages/0887-3585/suppmat/>

Grant sponsor: NIH; Grant numbers: DK36118, EY01677, GM71036, HL59378.

Ranvir Singh and Mark A. White contributed equally to this paper.

\*Correspondence to: Satish Srivastava, Department of Biochemistry and Molecular Biology, Room 6.644 Basic Science Building, UTMB, Galveston, TX 77555-0647. E-mail: [ssrivast@utmb.edu](mailto:ssrivast@utmb.edu)

The Atomic coordinates and structure factors (code 2F2K) have been deposited in the Protein Data Bank, Research Collaboratory for Structural Bioinformatics, Rutgers University, New Brunswick, NJ (<http://www.rcsb.org>).

Received 23 August 2005; Revised 7 February 2006; Accepted 20 February 2006

Published online 25 April 2006 in Wiley InterScience ([www.interscience.wiley.com](http://www.interscience.wiley.com)). DOI: 10.1002/prot.20988

generated by the oxidation of membrane lipids and lipoproteins<sup>9–11</sup> or during glucose<sup>12</sup> and amine<sup>13</sup> metabolism. Recently AR has also been shown to reduce core aldehydes that arise from the oxidation of unsaturated fatty acids esterified to the *sn*-2 position of phospholipids.<sup>14</sup> The role of this enzyme in aldehyde metabolism is supported by the observation that treatment with AR inhibitors increases inflammation- or ischemia-induced cardiovascular accumulation of 4-hydroxy-*trans*-2-nonenal (HNE), which is the major unsaturated aldehyde generated by lipid peroxidation.<sup>15,16</sup> Moreover, inhibition of AR has been shown to increase HNE-induced vascular smooth muscle cell death in culture,<sup>17,18</sup> indicating that this enzyme plays a key role in the detoxification of aldehydes generated by oxidized lipids.

A primary role of AR in aldehyde detoxification is consistent with its structure. The active site of the enzyme is highly hydrophobic and contains few polar residues required for binding sugars with high specificity and affinity.<sup>2,3</sup> These features are, however, compatible with binding to hydrophobic aldehydes such as those generated upon peroxidation of lipoproteins and membrane phospholipids. In addition, our studies show that the enzyme also catalyzes the reduction of the glutathione conjugates of unsaturated aldehydes; in most cases with efficiency greater than the reduction of the corresponding free aldehydes.<sup>19,20</sup> Studies with a variety of glutathione analogs suggest that both the N-terminal glutamate and the C-terminal glycine are specifically recognized and stabilized by the active-site residues of AR.<sup>19</sup> Nevertheless, the precise nature of glutathione binding to AR remained unclear. We therefore crystallized human AR bound to NADPH and  $\gamma$ -glutamyl-S-(1,2-dicarboxyethyl) cysteinylglycine (DCEG); a competitive inhibitor of the AR-catalyzed reaction of glutathionyl-propanal.<sup>19</sup> The crystal structure was determined to 1.94 Å, and revealed novel interactions between the glutathione backbone and active-site residues. Our results suggest that DCEG binding induces a significant conformational reorganization of the active site. This induced-fit rearrangement and the interactions near the AR active site with glutathione suggest a highly flexible glutathione-binding site.

## MATERIALS AND METHODS

### Overexpression and Purification of Recombinant Human AR

Recombinant human AR was overexpressed and purified as described earlier.<sup>22</sup> To purify the protein, bacterial extracts were subjected to chromatofocusing on PBE94 (Pharmacia LKB Biotechnology Inc.) followed by hydroxylapatite column chromatography and reactive blue affinity chromatography as the final step. All purification buffers contained 1 mM dithiothreitol (DTT).

### Crystallization of the Ternary Complex

Purified AR was concentrated by ultrafiltration (Amicon YM-10 membrane) to ~ 10 mg/mL. Prior to crystallization, 10 mg/mL AR in phosphate buffer (10 mM sodium phosphate pH 7.1, 0.5 mM EDTA, 10 mM DTT) was incubated

with NADPH and DCEG [ $\gamma$ -glutamyl-S-(1,2-dicarboxyethyl) glutathione; Fig. 1] at an AR:NADPH:DCEG molar ratio of 1:2:2 for 10 min at 4°C. The ternary complex was crystallized using the vapor diffusion method at 4°C. The protein:ligand solution was mixed with an equal volume of 22% (w/v) polyethylene glycol (PEG) 4000 in 100 mM sodium citrate (pH 5.0) + 50 mM magnesium sulphate and 6  $\mu$ L of droplets were placed above an identical well solution.

### Data Collection

X-ray data were collected using a MacScience DIP 2030H area detector and a M06XHF rotating anode X-ray generator operating at 50 kV and 90 mA equipped with Göbel collimating optics (Bruker AXS). The crystal,  $0.1 \times 0.1 \times 0.1$  mm<sup>3</sup>, was soaked in mother liquor containing 20% glycerol (v/v) and 25 mM of DCEG and was flash-cooled using 100 K nitrogen gas stream (Cryo Industries). The protein crystallized in the P2<sub>1</sub> monoclinic space group with cell dimensions  $a = 47.2$  Å,  $b = 66.7$  Å,  $c = 49.3$  Å,  $\alpha = \gamma = 90.0^\circ$ ,  $\beta = 92.2^\circ$ . This crystal form had not been observed previously for any AR crystal structures. Based upon the Matthews coefficient,<sup>23</sup> there was predicted to be one AR molecule per Ångstrom unit. The data were processed to 1.94 Å resolution using the program HKL.<sup>24</sup> Data collection and processing statistics are shown in Table I.

### Structure Determination and Refinement

The P2<sub>1</sub> crystal form structure was solved by molecular replacement using the program EPMR<sup>25</sup> with the AR: NADPH holoenzyme structure (1ADS<sup>3</sup>) as a search model. The PMB suite of programs<sup>27</sup> was used to generate a test set using 5% of the reflections chosen in thin shells equally spaced in 1/d. The PMB suite is as an interface to the structure refinement program CNS<sup>26</sup> that simplifies and partially automates the structure refinement process. Using PMB the variable sigma model of B-factor restraints<sup>28</sup> was implemented in CNS with parameters that are optimized to minimize the free R. In addition, PMB applied the optimal stereochemical bond root-mean-square deviation (RMSD) target of 0.015 Å, to automatically weight the X-ray terms in CNS. This target is based on an analysis of the ratio of free parameters to observations for several structures (data not shown). Application of both of these refinement targets in CNS led to a significant reduction in the free R value. The result is a model that has the least bias without overfitting of free parameters.<sup>29,30</sup> (The PMB software suite is available from <http://www.xray.utmb.edu/PMB>.) An initial rigid body refinement was followed by repetitive rounds of isotropic variable sigma B-factor and positional refinement, until the free R factor<sup>31</sup> no longer decreased. Then a round of simulated annealing was performed, and the results used only if the R<sub>free</sub> improved. The model was rebuilt in iterative rounds of model building (Xtalview<sup>32</sup>) and refinement. Parts of loop-B, residues 219 to 223, and the C-terminus were removed from the refinement model and rebuilt using omit maps. Structure factors were corrected

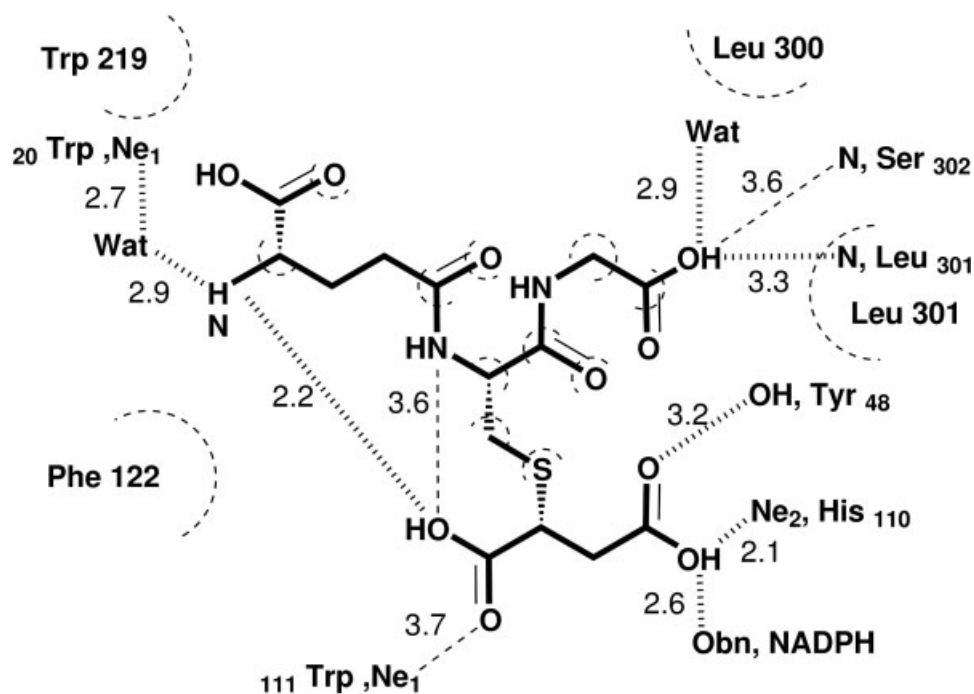


Fig. 1. Interactions of S-(1,2)-dicarboxyethyl glutathione with aldehyde reductase residues. Schematic representation of DCEG showing selected interactions between the inhibitor and the active site of the enzyme. Hydrogen bond and electrostatic interactions of the inhibitor with the protein or the solvent are shown as hatched lines. Distances, in angstroms, are given adjacent to the bonds. The dashed semicircles denote hydrophobic interactions with the protein. Note that the oxygens of the carboxyethyl arm of the inhibitor interact with the putative acid–base catalysts — His110 and Tyr48 and the C-terminal carboxylate interacts with Leu301 and Ser302.

for anisotropic scattering and absorption using the local scaling algorithm<sup>27,33,34</sup> in PMB. The DCEG inhibitor (Fig. 1) was modeled using Insight II (Accelrys, San Diego, CA) and energy minimized using the PRODRG web server,<sup>35</sup> which also generated the stereochemical restraints used in the structure refinement. Model building included the manual examination of waters selected by CNS, and rebuilding of all residues into omit maps. Waters with excessive B-factors ( $> 60 \text{ \AA}^2$ ) or poor density correlation were deleted. Model quality was assessed after each refinement step with XtalView or PROCHECK.<sup>36</sup> Refinement of the final model proceeded in parallel with alternate conformations of the DCEG ligand. The DCEG conformation with the best correlation with the electron density was chosen as the final model. This conformation also had the lowest free R. The DCEG ligand of this model produced the best fit to the electron density from the two separate refinements. (See Supplementary Material for details.) Multiple conformation refinement of DCEG in REFMAC,<sup>37,38</sup> including TLS anisotropic B-factors, with a single AR model and the two DCEG models confirmed that the chosen conformation had the highest correlation with the observations. Occupancy refinement in CNS revealed that the DCEG may be partially occupied, but its occupancy is at least 75%. Refinement at this occupancy lowered the B-factors for DCEG significantly. The final model used an occupancy of 1 for all atoms. All molecular figures were generated using PYMOL,<sup>39</sup> except for Figure 3 which was generated using XtalView and Raster3d.<sup>40</sup>

## RESULTS

The AR:NADPH:DCEG ternary complex structure was refined to 1.94 Å resolution with a final R factor of 19.6%, and  $R_{\text{free}}$  of 25.6%. The active site of AR is located at the base of a deep cleft or binding pocket. The sides of the active-site pocket are formed by three flexible loops, A, B, and C,<sup>41,42</sup> which are located on top of the AR ( $\alpha/\beta$ )<sub>8</sub> barrel [Fig. 2(A)]. The active site is comprised of residues Tyr48, His110, and Trp111. DCEG is bound at the active site almost filling the lower half of the active-site pocket. Trp219 and Phe122 form opposite sides of the narrow pocket holding the inhibitor DCEG [Fig. 2(C)]. The other residues lining this pocket include: Trp20, Trp79, Val47, Cys298, Ala299, Leu300, Leu301, and Ser302. The structure of AR in this complex is similar to that of the holoenzyme, except in the flexible loop regions, with an overall RMSD on  $\alpha$  carbons of 0.57 Å. The maximum observed  $C\alpha$  deviation in each of the three loops is 1.0, 5.2, and 0.5 Å for loops A, B, and C, respectively. The structure of AR with the DCEG inhibitor when compared with other inhibitors shows an overall RMSD of 0.25 to 0.68 Å, with the largest variations occurring in the three flexible loop regions [Fig. 2(B)]. The maximum observed  $C\alpha$  deviation in each of the three loops between the inhibitor structures listed in Figure 2(B) is 1.7, 1.3, and 1.8 Å for loops A, B, and C, respectively. Although these loops are flexible, able to adapt to accommodate inhibitors of varying size and shape, they do not display extreme dynamic behavior,

**TABLE I. Summary of Crystallographic Statistics**

PDB Accession id	2F2K
Space group	P2 <sub>1</sub>
Cell	
a (Å)	47.2
b (Å)	66.7
c (Å)	49.3
α (°)	90.0
β (°)	92.2
γ (°)	90.0
Data Collection	
Resolution range, Å	30–1.94
R <sub>merge</sub> , %	9.0 (30.7)
Unique observations	22,251
Average I/σ(I) <sup>a</sup>	13.8 (4.4)
Redundancy <sup>a</sup>	5.8 (3.2)
Completeness (%) <sup>a</sup>	97.7 (87.8)
Refinement Statistics	
R-factor (%) <sup>a</sup>	19.6 (24.5)
R <sub>free</sub> (%) <sup>a</sup>	25.6 (32.8)
RMS deviations	
Bonds (Å)	0.015
Angles (°)	1.8
Model Statistics	
No. residues in most-favored region	248
Additional allowed	27
Generously allowed	2
Disallowed	0
No. Atoms/average B factor (Å <sup>2</sup> )	
Protein Atoms	2517/20.8
NADPH	48/14.2
DCEG	28/77
Waters	159/23.7

<sup>a</sup>Values for the highest-resolution shells are given in parentheses.

their electron density is well defined, and they exhibit moderate B-factors.

The DCEG inhibitor is bound between two opposing surfaces in the active-site pocket, but does not completely fill the deep active-site cleft [Fig.2(C)]. The DCEG molecule makes ~ 80 contacts (defined as interresidue distances ≤ 4 Å) with residues in the active-site cleft (Fig. 1). The majority of these intermolecular contacts are hydrophobic. The NADPH binding site is located at the base of the AR hydrophobic active-site pocket and the nucleotide is bound to the ternary complex in an orientation identical to that observed in previously reported crystal structures.<sup>3,41,42</sup>

This structure shows well-defined electron density near the active site due to DCEG. The glutathione component appears to be dynamic or disordered, and does not have clear continuous electron density above 2 σ (Fig. 3). The DCEG in the crystal may not be fully occupied because occupancy refinement in CNS produced values of about 75% occupancy. However, given the moderate resolution of the data and the highly dynamic nature of the glutathione (GS) moiety compared to the dicarboxyethyl moiety that is strongly bound in the active site, these low occupancy values are probably driven by the overrestrained B-factors of the GS component. Due to the poorer density for the GS moiety, we attempted to fit the DCEG molecule into the

maps in different conformations. These included GS N- and C-terminal exchanged conformations, and models with the GS C-terminus bound in the active site. All these models left regions of the electron density unexplained, and extended significantly beyond the electron density contours for the ligand. (See Supplementary Material.)

Although the GS moiety of DCEG is highly dynamic, the orientation of the N- and C-termini of DCEG is the one that agrees best with the observed electron density. None of the other possible orientations, N- and C-termini flips or either terminus binding to the active site fit the electron density nearly as well as the one shown. These models do not fill the omit map density in the active site and extend beyond it. Furthermore, there is weak evidence, at 3 σ, in Bijvoet difference maps that the sulfur positions are consistent with our model (see Supplementary Material). A C-terminal peptide-flipped model with the GS peptide plane flipped between the Cys and Gly fits the density almost as well as our model. The peptide flipping, a 180° ψ rotation, moves the GS–cysteine from the β-sheet region to the α-helical region of ramachandran space. This rotation does not significantly alter the hydrogen bonding network shown in Figure 1. Occupancy refinement of these two models indicated that the original (β) model is the major conformer (65%), and that the peptide-flipped (α) conformation may exist as a minority species (23%). The occupancies are not restrained to total 100%. Although the electron density does not rule out alternate conformations, which are likely due to the disorder present in the GS moiety, the model shown represents the major conformation observed in the crystal. Omit maps of the electron density contoured below 3 σ do show the GS moiety and are most consistent with the DCEG orientation selected (see Supplementary Material). Our discussion of the DCEG structure will be limited to that of the major conformation.

The C-terminal glycine moiety of DCEG is hydrogen bonded to the backbone amides of Leu301 and Ser302 in the flexible AR C-terminal loop (loop-C); in addition, the ligand makes several van der Waals contacts with AR. The C-terminal carboxylate has weak electron density, indicating that its three possible hydrogen bonds may be partitioned between two alternate conformations of the C-terminal carboxylate. The C-terminal carboxylate shares hydrogen bonds with the backbone amides of Leu301 and Ser302. These residues are in AR loop-C which has been shown to be important for enzymatic activity. Mutations within this loop result in drastically lowered AR activity.<sup>44</sup> The N-terminus interacts with Trp20 indirectly through a water molecule. Two other waters, bound only to AR, fill parts of the active site not occupied by DCEG.

The dicarboxyethyl group of DCEG is anchored in the conserved anion binding site between the nicotinamide ring of NADPH and AR residues Tyr48, His110, and Trp111 similar to other known AR inhibitors.<sup>41,42</sup> The terminal carboxylates of the carboxyethyl are hydrogen bonded to active-site residues His110, Tyr48, and Trp111 (Fig. 3). The distal carboxylate is situated very near (2.6 Å) to the carboxylate of NADPH. This unfavorable interaction, similar to interactions observed in several other

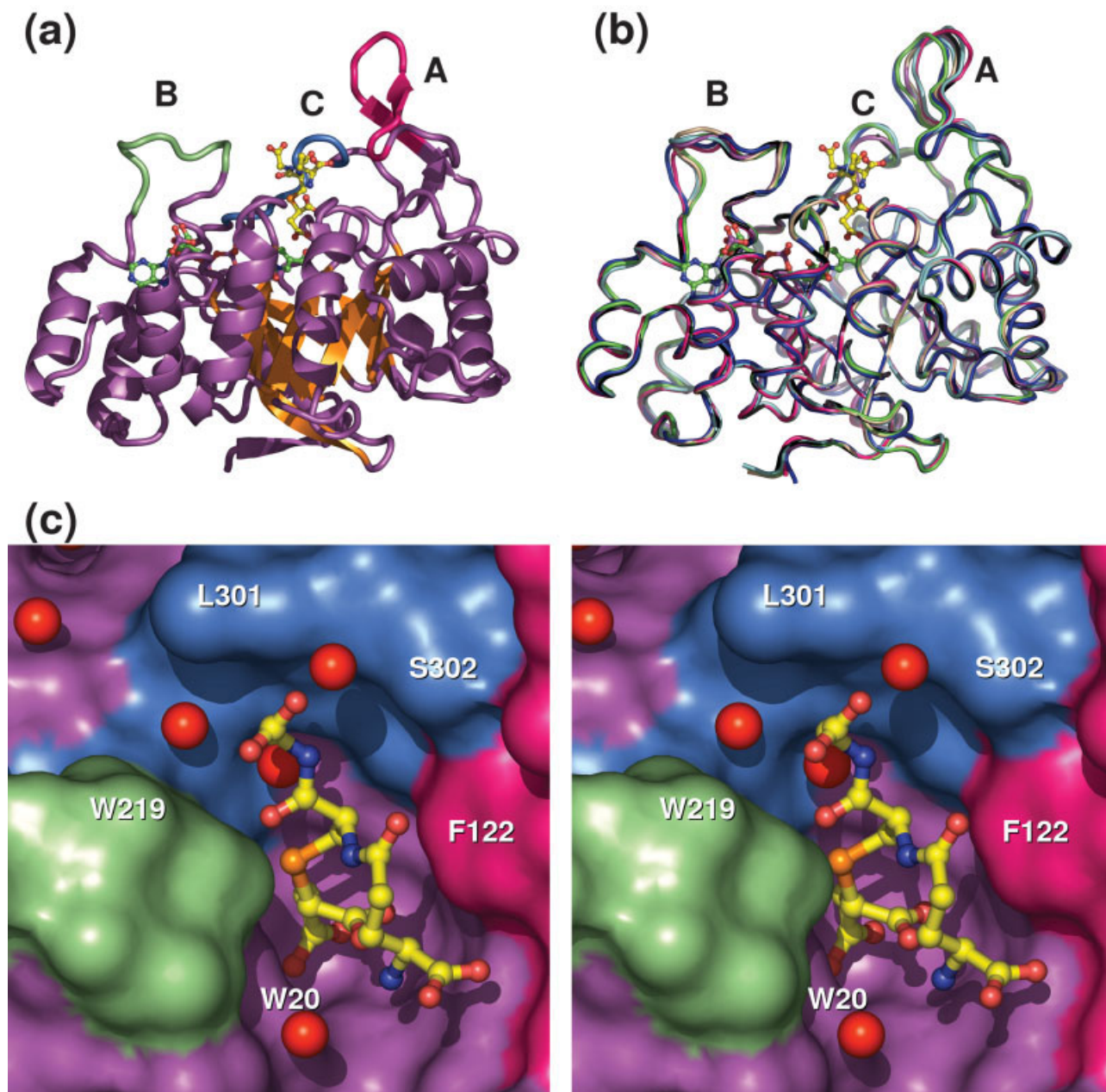


Fig. 2. The AR:NADPH:DCEG structure. **(A)** Ribbon drawing of the side view of the AR:NADPH (purple) binary complex bound to DCEG (shown as a yellow ball-and-stick model). The  $\beta$ -strands in the  $(\alpha/\beta)_8$  barrel are colored orange. The mobile active loops A, B, and C are colored red, green, and blue, respectively. **(B)** A comparison of several AR structures to AR:NADPH:DCEG (purple). The color-coded backbone trace of each structure is shown. The  $C\alpha$  RMSD to the DCEG complex is given in parentheses: red, holo (0.57 Å); cyan, glucose-6-phosphate (0.37 Å); beige, IDD384 (0.25 Å); blue, zenarestat (0.68 Å); green, minalrestat (0.45 Å); charcoal, fidarestat (0.25 Å); and yellow, IDD594 (0.30 Å). **(C)** A (cross-eyed) stereo-pair close-up view of DCEG (yellow ball-and-stick) and the two waters bound in the AR active site. The active-site residues, Tyr48, His110, Trp110, and NADPH, not labeled in this view, sit at the base of the deep active-site cleft where the DCEG dicarboxyethyl-moiety is bound.

inhibitors,<sup>41,42,48</sup> could be reduced by a flipping of the NADPH amide group (Obn in Fig. 1) concurrently with the flipping of the coordinating amide side-chain Asn160. The  $\gamma$ -glutamate of DCEG was observed to interact with AR through van der Waals contacts with Phe122 that forms one side of the hydrophobic active-site pocket and a water-mediated hydrogen bond with Trp20. The higher temperature factors for the  $\gamma$ -glutamate atoms reflect the relative disorder in the N-terminal end of DCEG. The

hydrophobic walls of the upper portion of the AR active-site pocket are formed in large part by Trp219 and Phe122, similar to the structure observed in other AR:inhibitor complexes.<sup>42,44</sup> These two aromatic residues tightly constrain the position of the cysteine moiety in DCEG. The Phe122 and Trp219 side-chains can move slightly to accommodate inhibitors of different size. The extensive hydrophobic interactions with Trp20 observed in the aromatic inhibitors tolrestat, zopolrestat, and sorbinil, are

completely absent in DCEG. The Trp20 and Trp79 residues, although still defining the active-site pocket, do not interact with DCEG directly. They do, however, limit the conformational space available to the DCEG molecule.

## DISCUSSION

The X-ray crystal structure of AR bound to DCEG reveals for the first time the structural basis for major interactions between the AR and glutathione conjugates suggested by previous kinetic, structure activity, and molecular modeling studies.<sup>19,20</sup> Our studies also show that AR catalyzes the reduction of the glutathione conjugates of unsaturated aldehydes in the heart, vascular smooth muscle cells, and erythrocytes,<sup>45,47</sup> suggesting that such conjugates may be *in vivo* substrates of AR. Because DCEG is a competitive inhibitor of AR with GS-propanal as the substrate,<sup>19</sup> this structure provides a detailed view of how substrate-like ligands affect the conformation of the protein that differs from its configuration when bound to product-like inhibitors (e.g., zopolrestat or sorbinil).

The conformation of protein in the present AR:NADPH:DCEG ternary complex structure is significantly different from that in the AR:NADPH binary complex.<sup>3</sup> The backbone atoms of Pro123 to Val131 in loop A and Pro218 to Pro225 in loop B, which flank the active-site pocket, are reoriented  $>5$  Å upon DCEG binding relative to the binary structure [Fig. 2(B)]. The AR:NADPH:DCEG ternary complex more closely resembles the AR:NADPH:zopolrestat<sup>48</sup> and AR:NADPH:IDD384<sup>41</sup> tertiary complexes than the AR:NADPH binary complex. In the ternary complexes the largest relative atomic movements, with RMSD  $> 1$  Å are in the region described by Ser127, Pro222, and Leu300. The conformation of loop B, residues Pro218 to Pro225, is very similar in all of the AR structures, with just the backbone conformation of residues Pro222 and Asp224 flipping in the holoenzyme. Loop A of the holoenzyme structure<sup>3</sup> displays a completely different conformation for this entire loop region relative to the current complex. Loop C adopts two different conformations, which depend upon the size and shape of the inhibitor bound to the protein. The conformation of loop C in the AR:NADPH:DCEG complex has the greatest similarity to the corresponding loop in the structure of AR:NADPH binary complex<sup>3</sup> and AR:NADPH:IDD384 ternary complex.<sup>41</sup> Additionally, loop C in the current structure has large positional differences with the conformation observed in the zopolrestat and tolrestat ternary complexes.<sup>42</sup> This indicates that loop C is flexible and is able to move to accommodate large molecules such as zopolrestat and tolrestat, whereas smaller inhibitors such as sorbinil do not change the conformation of this loop significantly.<sup>42</sup>

Based on molecular dynamics simulations of GS-propanal conjugate binding to AR,<sup>19</sup> we had proposed two possible alternate conformations of the glutathione conjugate bound to the active site. To constrain the orientation, the aldehyde function of the conjugate was positioned in the hydrophobic cleft with no steric clashes, such that the

carbonyl oxygen retains the geometry of the carboxylate of zopolrestat. In orientation 1, the N-terminal end of the conjugate faces the bottom of the barrel, with Glu1 of the conjugate between Lys21 and Trp20 and Gly3 of the conjugate in close proximity to the AR active-site residues Ser302 and Leu301. Alternately, in orientation 2, the  $\alpha$ -carboxylate group of Glu1 was positioned near the lip of the barrel whereas Gly3 at the C-terminus of the conjugate faces downwards and could hydrogen bond with Trp20, Val47, and Tyr48. Molecular modeling studies suggest that the interaction energy is greater in orientation 1 than in orientation 2. That orientation 1 is likely to be the preferred conformational state of the conjugate in the ternary complex is further substantiated by site-directed mutagenesis studies showing a much greater decrease in kinetic efficiency of Trp20Phe mutation with  $\gamma$ -Glu-Cys (propanal)-Gly than with  $\gamma$ -aminobutyric acid-Cys (propanal)-Gly as substrate suggesting stabilizing interactions between Trp20 and  $\alpha$ -carboxyl group of the conjugate. The current X-ray crystal structure of DCEG bound to AR also supports this model, replacing the direct interaction with an indirect interaction of the N-terminus with Trp20 through an intervening water molecule (Fig. 4). The observed binding of DCEG in the ternary complex is similar to orientation 1 of our molecular dynamics simulation (1.7 Å overall RMSD on the GS backbone, and 0.9 Å RMSD excluding the disordered N-terminus of the substrate). The variations between the model and DCEG structure could be attributed to the change in the active-site atoms from carbonyl in GS-propanal to  $\alpha$  carboxylate in DCEG, and the conformational freedom of the  $\gamma$ -glu N-terminus. The bulkier dicarboxyethyl moiety seems to have pushed the GS backbone further away from the active site than in the propanal-GS model. The C-terminal hydrogen bonds to Leu301 and Ser302 are maintained, while the N-terminal hydrogen bond with Trp20 is not seen in the crystal structure. Instead, the N-terminal of DCEG is hydrogen bonded to the dicarboxyethyl group and to a water molecule bound to Trp20.

We have shown previously that DCEG is a competitive inhibitor of the reduction of glutathionated aldehydes by AR,<sup>19</sup> indicating that the conjugate binds selectively to the AR:NADPH binary complex and has little or no affinity for the AR:NADP<sup>+</sup> complex. Reasons for this selectivity are apparent from the current structure. The nonspecific interactions of DCEG with the active-site cleft, and the loose shape complementarity are consistent with a very low affinity of DCEG for apo AR. The result of NADPH binding is to rearrange the active-site residues Tyr48, His110, and Trp111, plus the adjacent A, B, and C loops. Thus, NADPH binding orientates these regions to form the active-site pocket. It is only after these rearrangements that AR would have any significant affinity for DCEG. Therefore, DCEG binding must be preceded by the formation of the AR:NADPH binary complex. Moreover, in the AR:NADPH:DCEG ternary complex, a larger percentage (50%) of DCEG is buried by AR side chains than has been observed in structures of other GS-binding proteins (40%–45%),

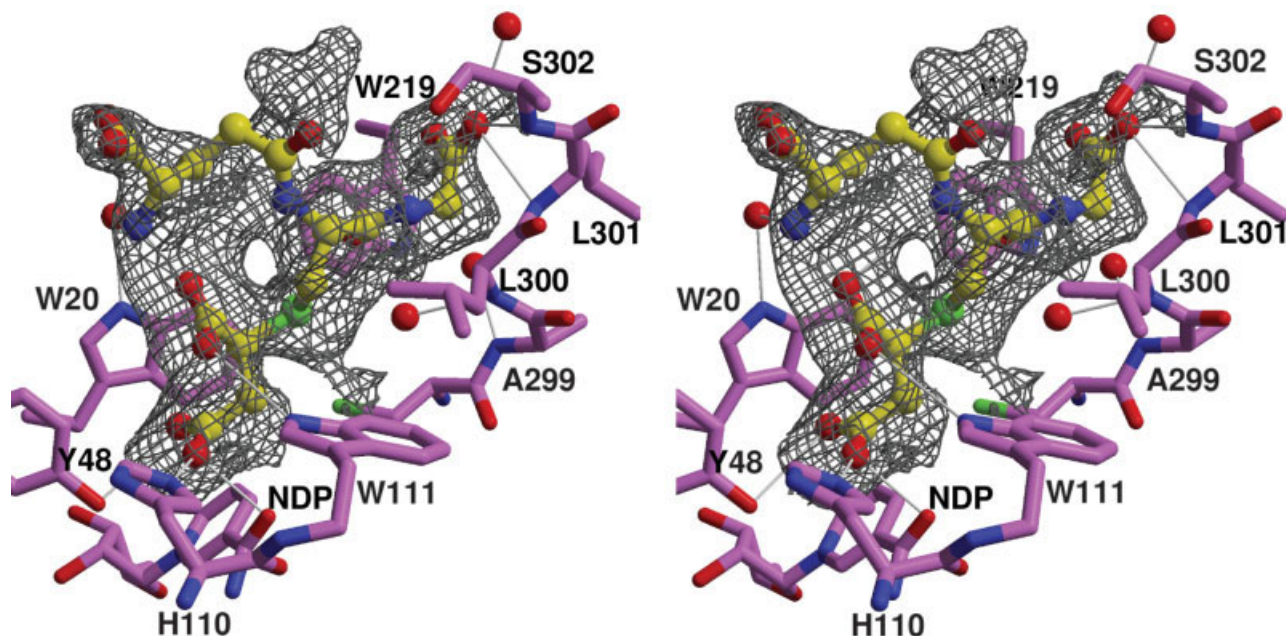


Fig. 3. DCEG binding to the AR active site. A (cross-eye) stereo-pair side view of the AR active site, looking from Phe122, not shown, toward Trp219. The DCEG (yellow) and active-site waters are shown as ball-and-stick. The AR:NADPH active-site residues are in purple stick representation. The sigma-A weighted (Fo-Fc) omit map (gray) is contoured at  $2\sigma$ . Hydrogen bonds and electrostatic interactions are drawn as thin white lines. In this view the binding of the inhibitor to the active-site residues, Tyr48, His110, Trp110, and NADPH, is shown clearly, as are the C-terminal carboxylate interactions with Leu301 and Ser302.

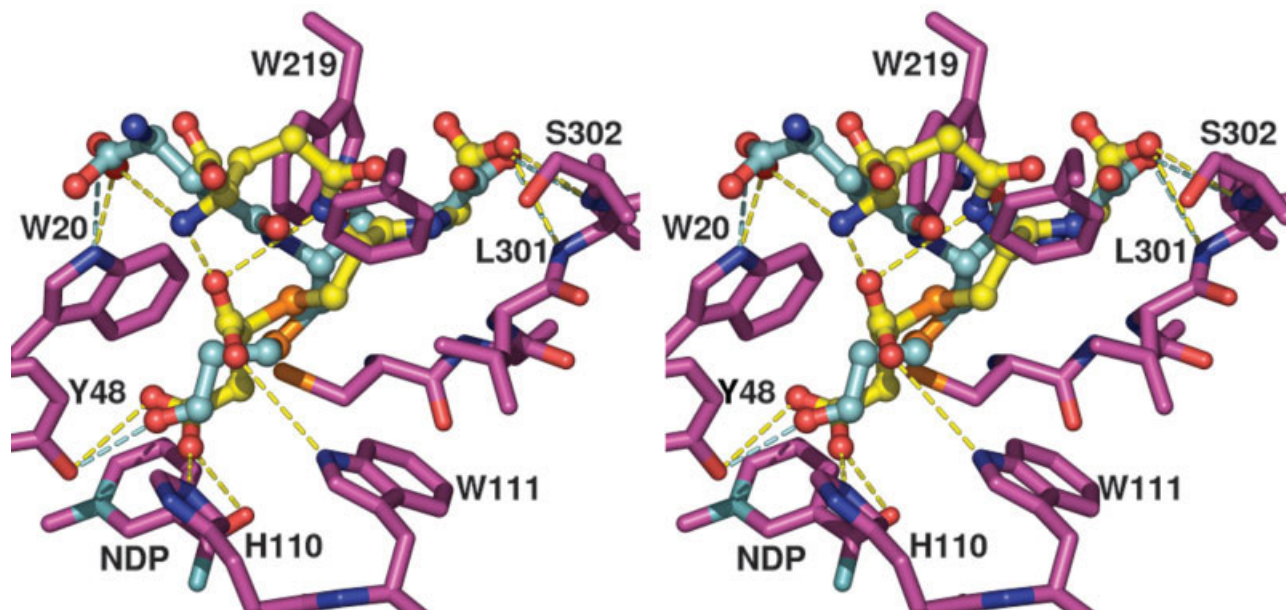


Fig. 4. A comparison of the propanol-GS model with DCEG. A (cross-eye) stereo-pair view of the molecular dynamics model of propanol-GS (cyan) binding to the holo-enzyme in comparison with the AR:NADPH:DCEG structure (yellow). Hydrogen bonds are shown as yellow or cyan dashes for DCEG or propanol-GS, respectively. The two ligands share several common modes of interaction. The slightly shorter propanol-GS molecule still uses the C-terminal carboxylate interactions with the C loop Leu31 and Ser302 residues to stabilize the GS moiety. The labile water mediated N-terminal hydrogen bond with Trp20 and the active-site interactions are the only intermolecular hydrogen bonds. The two GS conjugates illustrate the flexibility of GS conjugate binding to AR and its specificity in loop C.

suggesting that the strongly aliphatic nature of DCEG, which allows multiple contacts at the active site, is essential for competitive inhibition of glutathionyl-aldehyde reduction, due to selective binding to the AR:NADPH binary complex. In contrast, more aromatic

inhibitors, which bind to the AR active site primarily via hydrophobic interactions, bind with greater affinity to the AR:NADP<sup>+</sup> binary complex and thus behave as noncompetitive inhibitors of aldehyde reduction, but competitive inhibitors of alcohol oxidation.<sup>19</sup>

Our previous comparisons between steady-state kinetic parameters of the enzyme for glutathiolated and free aldehydes show that glutathiolation enhances the overall catalytic efficiency of aldehyde reduction by AR.<sup>19,20</sup> The AR:NADPH:DCEG structure provides direct evidence for the reason behind this enhancement of catalytic efficiency. In addition to dramatically increasing the nonspecific hydrophobic interactions within the binding pocket, the C-terminus of the glutathione has hydrogen bond interactions with AR. The flexibility provided by these interactions suggests that the contribution of glutathione to the binding energy can vary with the shape and size of the conjugated moiety. The glutathione conjugates may rotate around the C-terminal hydrogen bonds and still provide significant, but possibly different, hydrophobic interactions with the walls of the binding pocket, thus permitting a variety of glutathione conjugates to bind to the AR active site. This is clearly demonstrated by the examples of nonanal and propanal reduction. The glutathiolated forms of these aldehydes display 5- and 1360-fold higher catalytic efficiency, respectively, than the corresponding free aldehyde. The current structure suggests that this dramatic increase in catalytic efficiency likely results from the observed interactions with AR, the hydrogen bonds with Leu301 and S302, the hydrophobic interactions with Phe122 and Trp219, and an entropic effect of the intramolecular hydrogen bonds. Although glutathione by itself binds poorly to the enzyme ( $K_i = 1.5 \text{ mM}$ ), the combined configuration of the conjugate adopts a favorable conformation at the active site, improving the catalytic efficiency by modifying both  $K_{\text{cat}}$  and  $K_m$ . This effect is expected depending on the size of the conjugate, as observed for our GS–propanal model and DCEG structure. The hydrogen bond interactions will be strained, and the hydrophobic interactions shifted as the GS backbone moves relative to AR to accommodate different conjugates.

In contrast to its folded structure in solution, glutathione adopts an extended configuration when bound to the active site of proteins, usually assuming a Y or a V shape. The conformation of the glutathione moiety of the AR-bound DCEG [Fig. 2(C)] was similar to the Y form conformation of glutathione observed in the GS-binding proteins glutathione-S-transferase,<sup>49</sup> sphingomonad GST (1F2E<sup>50</sup>), human thioltransferase,<sup>51</sup> yeast prion Ure2p,<sup>52</sup> and the chloride intercellular channel.<sup>53</sup> The glutathione backbone conformation of DCEG was most distinct from the V-form conformation of glutathione bound to glutaredoxin (1b4q<sup>51</sup>) or glutathione reductase (1gra, 1gre<sup>55</sup>). Our molecular modeling studies suggested that the conformation of glutathione bound to the active site of AR resembles the Y configuration of the molecule (Fig. 4). This is supported by the current crystal structure showing that the glutathione backbone of DCEG bound to AR adopts the low energy Y shape, rather than the V form of GS observed in glutaredoxin,<sup>51</sup> glutathione reductase,<sup>54,55</sup> and glutathione peroxidase<sup>56</sup> complexes. The glutathione backbone of DCEG overlaps with these glutathione structures with RMSD from 0.4 to 1.4 Å. The largest RMSD between the observed structures of glutathione bound to several differ-

ent enzymes and DCEG bound to AR occurred in the N- and C-terminal atoms. In comparison with glutathione bound to glutaredoxin, the cysteine of DCEG bound to AR has a  $\phi$  angle that is rotated by  $\sim 180^\circ$ . The AR-bound DCEG glutathione backbone conformation is most similar to that observed in GS complexes with hematopoietic prostaglandin D synthase<sup>57</sup> or yeast prion Ure2p.<sup>52</sup> DCEG binding to AR lacks the N-terminal hydrogen bonds seen in the other GS:protein complexes. The placement of the glutathione backbone is largely determined by the interaction of the conjugate with the active site of the enzyme and the mobile loop C. The hydrophobic interactions with the binding cleft are nonspecific and allow for flexibility of the GS moiety.

The structure of DCEG bound to AR provides a starting model for understanding how the binding of free aldehydes and aldehyde–glutathione conjugates could be differentially affected either physiologically or pharmacologically. In this structure only a few specific interactions of the DCEG glutathione moiety with AR were observed indicating that it is unlikely that GS-conjugate binding could be perturbed without affecting the binding of free aldehydes as well. The majority of the binding affinity appears to be associated with binding to the AR active site. The GS specific binding is limited to the backbone of loop C, and nonspecific hydrophobic interactions with the walls of the active-site cleft. However, our previous studies have shown site-directed mutations at the glutathione-binding site (Ser302 and Trp20) selectively diminishes the catalytic efficiency of the enzyme with aldehyde–glutathione conjugates without affecting the efficiency for the reduction of free aldehydes.<sup>20</sup> This observation along with current structure indicate that steric hindrance of part of the GS binding site, such as loop-C, would prevent GS-conjugates and larger molecules from reaching the active site. It further suggests the possibility that pharmacologic or endogenous ligands affecting the movement of this loop could alter the relative affinity of the enzyme for aldehyde–glutathione conjugates and free aldehydes. Loop C is located at one end of the opening to the active-site cleft, which is approximately  $6 \times 15 \text{ \AA}$  wide and  $10 \text{ \AA}$  deep. Part of this opening could be partially blocked without preventing small aldehydes from reaching the active site, and thereby selectively affecting the binding of glutathione conjugates. Such interventions would allow testing of the relative role of AR in glutathione conjugate metabolism and aldehyde detoxification.

In summary, we have shown how DCEG, a glutathione-conjugated carboxylate, binds to AR. The carboxylate function of the molecule binds at the AR active site, while the C-terminus of the glutathione backbone of the conjugate binds to the AR loop C. This structure provides insights into the mechanism by which glutathiolation enhances catalytic efficiency of aldehyde reduction by AR, and offers the possibility of selectively inhibiting the binding and reduction of glutathione-conjugated aldehydes, while still retaining the capacity of the enzyme to detoxify free cytotoxic aldehydes. The structure of the AR:NADPH:DCEG complex shows for the first time effi-

cient binding of glutathione to a protein in a noncatalytic role.

### ACKNOWLEDGMENTS

We thank Sealy and Smith Foundation for supporting M.A.W., and the Sealy Center for Structural Biology and NIEHS ESO6676-11 grant supported core facilities.

### REFERENCES

1. Jez JM, Bennett MJ, Schlegel BP, Lewis M, Penning TM. Comparative anatomy of the aldo-keto reductase superfamily. *Biochem J* 1997;326:625–636.
2. Rondeau JM, Tete-Favier F, Podjarny A, Reymann JM, Barth P, Biellmann JF, Moras D. Novel NADPH-binding domain revealed by the crystal structure of aldose reductase. *Nature* 1992;355:469–472.
3. Wilson DK, Bohren KM, Gabbay KH, Quiocho FA. An unlikely sargur substrate in the 1.65 Å structure of the human aldose reductase holoenzyme implicated in diabetic complications. *Science* 1992;257:81–84.
4. Bhatnagar A, Srivastava SK. Aldose reductase: congenial and injurious profiles of an enigmatic enzyme. *Biochem Med Metab Biol* 1992;48:91–121.
5. Burg MB. Role of aldose reductase and sorbitol in maintaining the medullary intracellular milieu. *Kidney Int* 1998;33:635–641.
6. Petrash JM, Tarle I, Wilson DK, Quiocho FA. Aldose reductase catalysis and crystallography. Insights from recent advances in enzyme structure and function. *Diabetes* 1994;43:955–959.
7. Sheetz MJ, King GL. Molecular understanding of hyperglycemia's adverse effects for diabetic complications. *JAMA* 2002;288:2579–2588.
8. Parry GJ. Management of diabetic neuropathy. Management of diabetic neuropathy. *Am J Med* 1999;107:27S–33S.
9. Srivastava S, Chandra A, Bhatnagar A, Srivastava SK, Ansari NH. Lipid peroxidation product, 4-hydroxynonenal and its conjugate with GSH are excellent substrates of bovine lens aldose reductase. *Biochem Biophys Res Commun* 1995;217:741–746.
10. Srivastava S, Chandra A, Ansari NH, Srivastava SK, Bhatnagar A. Identification of cardiac oxidoreductase(s) involved in the metabolism of the lipid peroxidation-derived aldehydes-4-hydroxynonenal. *Biochem J* 1998;329:469–475.
11. Srivastava S, Watowich SJ, Petrash JM, Srivastava SK, Bhatnagar A. Structural and kinetic determinants of aldehydes reduction by aldose reductase. *Biochemistry* 1999;38:42–54.
12. Vander Jagt DL, Robinson B, Taylor KK, Hunsaker LA. Reduction of trioses by NADPH-dependent aldo-keto reductases. Aldose reductase, methylglyoxal, and diabetic complications. *J Biol Chem* 1992;267:4364–4369.
13. Kawamura M, Eisenhofer G, Kopin IJ, Kador PF, Lee YS, Tsai JY, Fujisawa S, Lizak MJ, Sinz A, Sato S. Aldose reductase, a key enzyme in the oxidative deamination of norepinephrine in rats. *Biochem Pharmacol* 1999;58:517–524.
14. Srivastava S, Spite M, Trent JO, West MB, Ahmed Y, Bhatnagar A. Aldose reductase-catalyzed reduction of aldehydes phospholipids. *J Biol Chem* 2004;279:53395–53406.
15. Rittner HL, Hafner V, Klimiuk PA, Szweda LI, Goronzy JJ, Weyand CM. Aldose reductase functions as a detoxification system for lipid peroxidation products in vasculitis. *J Clin Invest* 1999;103:1007–1013.
16. Shinmura K, Bolli R, Liu SQ, Tang XL, Kodani E, Xuan YT, Srivastava S, Bhatnagar A. Aldose reductase is an obligatory mediator of the late phase of ischemic preconditioning. *Circ Res* 2002;91:240–246.
17. Ruef J, Liu SQ, Bode C, Tocchi M, Srivastava S, Runge MS, Bhatnagar A. Involvement of aldose reductase in vascular smooth muscle cell growth and lesion formation after arterial injury. *Arterioscler Thromb Vasc Biol* 2000;20:1745–1752.
18. Ramana KV, Chandra D, Srivastava S, Bhatnagar A, Aggarwal BB, Srivastava SK. Aldose reductase mediates Mitogenic signaling in vascular smooth muscle cells. *J Biol Chem* 2002;277:32063–32070.
19. Dixit BL, Balendiran GK, Watowich SJ, Srivastava S, Ramana KV, Petrash JM, Bhatnagar A, Srivastava SK. Kinetic and structural characterization of the glutathione-binding site of aldose reductase. *J Biol Chem* 2000;275:21587–21595.
20. Ramana KV, Dixit BL, Srivastava S, Balendiran GK, Srivastava SK, Bhatnagar A. Selective recognition of glutathiolated aldehydes by aldose reductase. *Biochemistry* 2000;39:12172–12180.
21. Ramana KV, Bhatnagar A, Srivastava SK. Inhibition of aldose reductase attenuates TNF- $\alpha$ -induced expression of adhesion molecules in endothelial cells. *FASEB J* 2004;18:1209–1218.
22. Petrash JM, Harter TM, Devine CS, Olins PO, Bhatnagar A, Liu S, Srivastava SK. Involvement of cysteine residues in catalysis and inhibition of human aldose reductase. Site-directed mutagenesis of Cys-80, -298, and -303. *J Biol Chem* 1992;267:24833–24840.
23. Matthews BW. Solvent content of protein crystals. *J Mol Biol* 1962;33:491–497.
24. Otwinowski Z, Minor W. Processing of X-ray diffraction data collected in oscillation mode. *Meth Enz* 1997;276:307–326.
25. Kissinger CR, Gehlhaar DK, Smith BA, Bouzida D. Molecular replacement by evolutionary search. *Acta Crystallogr D Biol Crystallogr* 2001;57:1474–1479.
26. Brunger AT, Adams PD, Clore GM, DeLano WL, Gros P, Grosse-Kunstleve RW, Jiang JS, Kuszewski J, Nilges M, Pannu NS, Read RJ, Rice LM, Simonson T, Warren GL. Crystallography & NMR system: a new software suite for macromolecular structure determination. *Acta Crystallogr D Biol Crystallogr* 1998;54:905–921.
27. Scott EE, White MA, He YA, Johnson EF, Stout CD, Halpert JR. Structure of mammalian cytochrome P450 2B4 complexed with 4-(4-chlorophenyl) imidazole at 1.9-Å resolution: insight into the range of P450 conformations and the coordination of redox partner binding. *J Biol Chem* 2004;279:27294–27301.
28. Tickle IJ, Laskowski RA, Moss DS. Error estimates of protein structure coordinates and deviations from standard geometry by full-matrix refinement of gammaB- and betaB2-crystallin. *Acta Crystallogr D Biol Crystallogr* 1998;54:243–252.
29. Tickle IJ, Laskowski RA, Moss DS. Rfree and the rfree ratio. I. Derivation of expected values of cross-validation residuals used in macromolecular least-squares refinement. *Acta Crystallogr D Biol Crystallogr* 1998;54:547–557.
30. Tickle IJ, Laskowski RA, Moss DS. Rfree and the rfree ratio. II. Calculation of the expected values and variances of cross-validation statistics in macromolecular least-squares refinement. *Acta Crystallogr D Biol Crystallogr* 2000;56:442–450.
31. Brunger AT. The free R value: a novel statistical quantity for assessing the accuracy of crystal structures. *Nature* 1992;355:472–474.
32. McRee DE. Xtal View/Xfit — a versatile program for manipulating atomic coordinates and electron density. *J Struct Biol* 1999;125:156–165.
33. Matthews B, Czerwinski E. Local scaling: a method to reduce systematic errors in isomorphous replacement and anomalous scattering measurements. *Acta Crystallogr* 1975;A31:480–487.
34. Hynes TR, Fox RO. The crystal structure of staphylococcal nuclease refined at 1.7 Å resolution. *Proteins* 1991;10:92–105.
35. van Aalten DM, Bywater R, Findlay JB, Hendlich M, Hooff RW, Vriend G. PRODRG, a program for generating molecular topologies and unique molecular descriptors from coordinates of small molecules. *J Comp Mol Design* 1996;10:255–262.
36. Laskowski R, Rullmann J, MacArthur M, Kaptein R, Thornton J. AQUA and PROCHECK-NMR: programs for checking the quality of protein structures solved by NMR. *J Biomol NMR* 1996;8:477–486.
37. Murshudov GN, Vagin AA, Lebedev A, Wilson KS, Dodson EJ. Efficient anisotropic refinement of macromolecular structures using FFT. *Acta Crystallogr D Biol Crystallogr* 1999;55:247–255.
38. Collaborative Computational Project Number 4, *Acta Cryst D* 1994;50:760–763.
39. Delano WL. The PyMOL molecular graphics system. Delano Scientific, San Carlos, CA: Delano Scientific; 2003.
40. Merritt EA, Bacon DJ. Raster3D photorealistic molecular graphics. *Meth Enzymol* 1997;277:505–524.
41. Calderone V, Chevrier B, Van Zandt M, Lamour V, Howard E, Poterszman A, Barth P, Mitschler A, Lu J, Dvornik DM, Klebe G, Kraemer O, Moorman AR, Moras D, Podjarny A. The structure of human aldose reductase bound to the inhibitor IDD384. *Acta Crystallogr D Biol Crystallogr* 2000;56:536–540.
42. Urzhumtseva L, Tete-Favier F, Mitschler A, Barbantoni J, Barth P, Urzhumtseva L, Biellmann JF, Podjarny A, Moras D. A specificity pocket inferred from the crystal structures of the complexes of

- aldose reductase with the pharmaceutically important inhibitors tolrestat and sorbinil. *Structure* 1997;5:601–612.
43. El-Kabbani O, Wilson DK, Petrash M, Quioco FA. Structural features of the aldose reductase and aldehydes reductase inhibitor-binding sites. *Mol Vis* 1998;4:19–25.
  44. Bohren KM, Grimshaw CE, Gabbay KH. Catalytic effectiveness of human aldose reductase. Critical role of C-terminal domain. *J Biol Chem* 1992;267:20965–20970.
  45. Srivastava S, Chandra A, Wang LF, Seifert WE Jr, DaGue BB, Ansari NH, Srivastava SK, Bhatnagar A. Metabolism of the lipid peroxidation product, 4-hydroxy-trans-2-nonenal, in isolated perfused rat heart. *J Biol Chem* 1998;273:10893–10900.
  46. Srivastava S, Conklin DJ, Liu SQ, Prakash N, Boor PJ, Srivastava SK, Bhatnagar A. Identification of biochemical pathways for the metabolism of oxidized low-density lipoprotein derived aldehyde-4-hydroxyl trans-2-nonenal in vascular smooth muscle cells. *Atherosclerosis* 2001;158:339–350.
  47. Srivastava S, Dixit BL, Cai J, Sharma S, Hurst HE, Bhatnagar A, Srivastava SK. Metabolism of lipid peroxidation product, 4-hydroxynonenal (HNE) in rat erythrocytes: role of aldose reductase. *Free Radic Biol Med* 2000;29:642–651.
  48. Wilson DK, Tarle I, Petrash JM, Quioco FA. Refined 1.8 Å structure of human aldose reductase complexed with the potent inhibitor zopolrestat. *Proc Natl Acad Sci U S A* 1993;90:9847–9851.
  49. Prade L, Huber R, Manoharan TH, Fahl WE, Reuter W. Structures of class pi glutathione S-transferase from human placenta in complex with substrate, transition-state analogue and inhibitor. *Structure* 1997;5:1287–1295.
  50. Sussman JL, Lin D, Jiang J, Manning NO, Prilusky J, Ritter O, Abola EE. Protein Data Bank (PDB): database of three-dimensional structural information of biological macromolecules. *Acta Crystallogr. D Biol Crystallogr.* 1998;54:1078–1084.
  51. Yang Y, Jao S, Nanduri S, Starke DW, Mieyal JJ, Qin J. Reactivity of the human thioltransferase (glutaredoxin) C7S, C25S, C78S, C82S mutant and NMR solution structure of its glutathionyl mixed disulfide intermediate reflect catalytic specificity. *Biochemistry* 1998;37:17145–17156.
  52. Bousset L, Belrhali H, Melki R, Morera S. Crystal structures of the yeast prion Ure2p functional region in complex with glutathione and related compounds. *Biochemistry* 2001;40:13564–13573.
  53. Harrop SJ, DeMaere MZ, Fairlie WD, Reztsova T, Valenzuela SM, Mazzanti M, Tonini R, Qiu MR, Jankova I, Warton K, Bauskin AR, Wu WM, Pankhurst S, Campbell TJ, Breit SN, Curmi PM. Crystal structure of a soluble form of the intracellular chloride ion channel CLIC1 (NCC27) at 1.4-Å resolution. *J Biol Chem* 2001;276:44993–45000.
  54. Becker K, Savvides SN, Keese M, Schirmer RH, Karplus PA. Enzyme inactivation through sulfhydryl oxidation by physiologic NO-carriers. *Nat Struct Biol* 1998;5:267–271.
  55. Karplus PA, Pai EF, Schulz GE. A crystallographic study of the glutathione binding site of glutathione reductase at 0.3-nm resolution. *Eur J Biochem* 1989;178:693–703.
  56. Epp O, Ladenstein R, Wendel A. The refined structure of the selenoenzyme glutathione peroxidase at 0.2-nm resolution. *Eur J Biochem* 1983;133:51–69.
  57. Kanaoka Y, Ago H, Inagaki E, Nanayama T, Miyano M, Kikuno R, Fujii Y, Eguchi N, Toh H, Urade Y, Hayaishi O. Cloning and crystal structure of hematopoietic prostaglandin D synthase. *Cell* 1997;90:1085–1095.